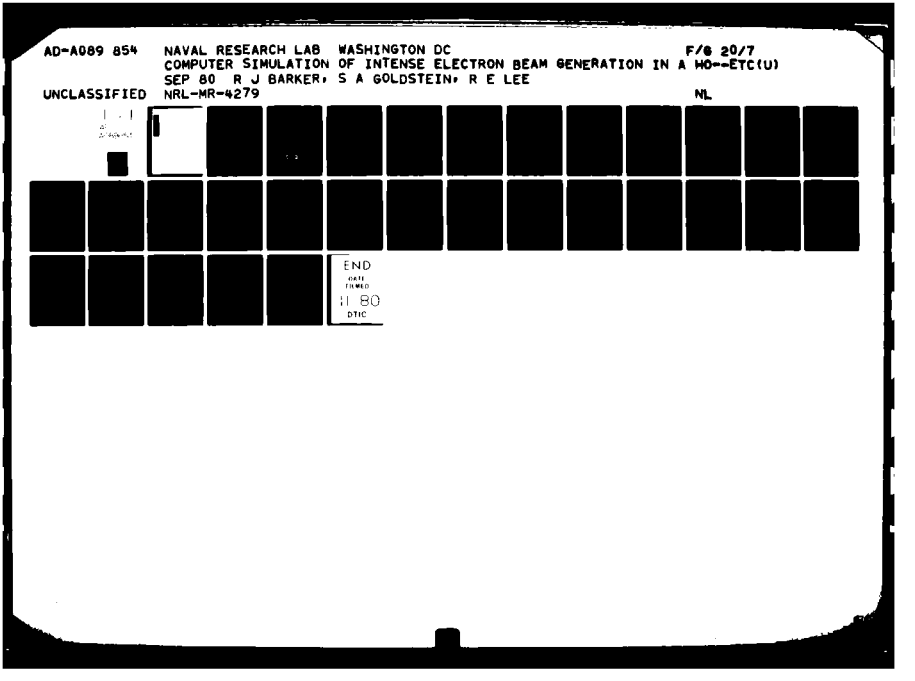
AD-A089 854
NAVAL RESEARCH LAB WASHINGTON DC
F/6 20/7
COMPUTER SIMULATION OF INTENSE ELECTRON BEAM GENERATION IN A HO--ETC(U)
SEP 80 R J BARKER, S A GOLDSTEIN, R E LEE
UNCLASSIFIED
NRL-MR-4279
NL
END
DATE FILMED
11-80
DTIC

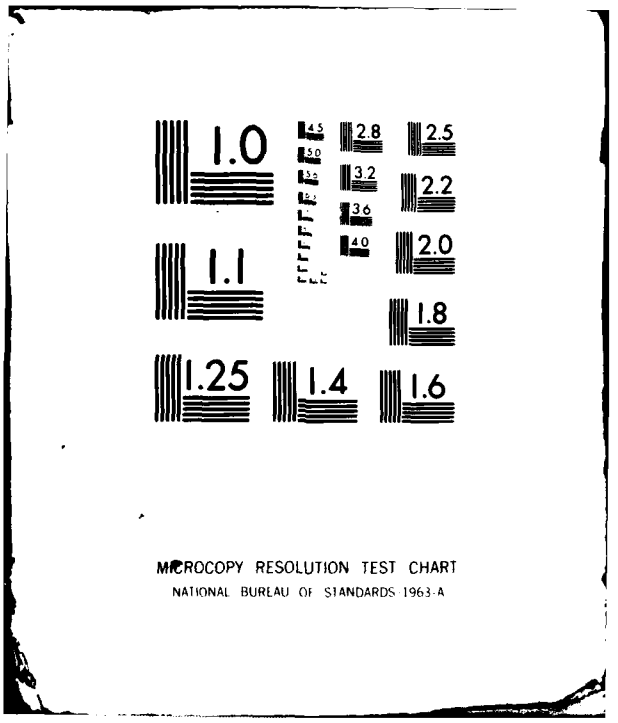
1.0
1.1
1.25
1.4
1.6
1.8
2.0
2.2
2.5
2.8
3.2
3.6
4.0
4.5
5.0
MICROCOPY RESOLUTION TEST CHART
NATIONAL BUREAU OF STANDARDS 1963-A

(14) NRL-MR-4279

SECURITY CLASSIFICATION OF THIS PAGE (When Data Entered)

REPORT DOCUMENTATION PAGE

READ INSTRUCTIONS BEFORE COMPLETING FORM

1. REPORT NUMBER: NRL Memorandum report 4279
2. GOVT ACCESSION NO.: AD-A089854
3. RECIPIENT'S CATALOG NUMBER
(9) Memorandum report

4. TITLE (and Subtitle): (6) COMPUTER SIMULATION OF INTENSE ELECTRON BEAM GENERATION IN A HOLLOW CATHODE DIODE
5. TYPE OF REPORT & PERIOD COVERED: Interim report on a continuing project June — December 1978
6. PERFORMING ORG. REPORT NUMBER

7. AUTHOR(s): (10) R. J. Barker* Shyke A. Goldstein** and Roswell E. Lee**
8. CONTRACT OR GRANT NUMBER(s)

9. PERFORMING ORGANIZATION NAME AND ADDRESS
Naval Research Laboratory
Washington, D. C. 20375

10. PROGRAM ELEMENT, PROJECT, TASK AREA & WORK UNIT NUMBERS
67-0879-0-0

11. CONTROLLING OFFICE NAME AND ADDRESS
Department of Energy
Washington, D.C. 20545
(11) 5

12. REPORT DATE
September 1980
13. NUMBER OF PAGES
30

14. MONITORING AGENCY NAME & ADDRESS (if different from Controlling Office)
(12) 31

15. SECURITY CLASS. (of this report)
UNCLASSIFIED

15a. DECLASSIFICATION/DOWNGRADING SCHEDULE

16. DISTRIBUTION STATEMENT (of this Report)

Approved for public release, distribution unlimited.

17. DISTRIBUTION STATEMENT (of the abstract entered in Block 20, if different from Report)

18. SUPPLEMENTARY NOTES

*Work performed while an NRL/NRC Postdoctoral Research Associate.
Present address: JAYCOR, Alexandria, VA 22304
**Present address: JAYCOR, Alexandria, VA 22304

19. KEY WORDS (Continue on reverse side if necessary and identify by block number)

Hollow cathode diode
Computer simulation
Relativistic electron beam

20. ABSTRACT (Continue on reverse side if necessary and identify by block number)

A modified version of NRL's DIODE2D computer simulation code is used to model the electron and proton flow in a hollow cathode diode. Results correspond closely to those observed in experiments performed at NRL and give direct insight into the diode physics. The strong dependence of diode performance on two-dimensional distortions of the A-K gap electric field as well as upon the presence of a strong axial magnetic field is clearly illustrated.

DD FORM 1 JAN 73 1473 EDITION OF 1 NOV 65 IS OBSOLETE
S/N 0102-LF-014-6601

251950

SECURITY CLASSIFICATION OF THIS PAGE (When Data Entered)

TABLE OF CONTENTS

COMPUTER SIMULATION OF INTENSE ELECTRON BEAM GENERATION IN A HOLLOW CATHODE DIODE

Introduction

Several years ago at the Naval Research Laboratory, Cooperstein, et al., observed some interesting anode damage patterns during runs of the Gamble I low-impedance diode.[1] The experimental arrangement is depicted in Fig. 1. A simple carbon hollow cathode opposed a flat plate porous graphite anode. (Note that only the small D carbon witness plate location is of interest here.) Large external magnetic field coils maintained the entire configuration in a 30 kG solenoidal magnetic field. A number of discharges were run in the 600 kV to 1 MV range. After a typical experiment, examination revealed that a perfect circular groove had been cut into the anode surface. The dimensions of the groove were such that the cathode could neatly fit into it. Furthermore, upon closer examination there was an even finer pattern of damage inside the groove. A radial cross-section had the shape of a straight-sided "W". The groove was decidedly deeper at the edges than along the center.

The close correspondence between the cathode radius and the damage radius was attributed to the effect of the strong axial magnetic field. This effect alone, however, could not explain the sheer magnitude of the damage. Some 100 kA/cm^2 of electron current density would have been required to pulverize the anode material. Standard one-dimensional analysis cannot explain the emission of such high current densities from the cathode.

Manuscript submitted June 16, 1980

Nevertheless, their existence has been established. A possible explanation is that electron emission is enhanced through a two-dimensional intensification of the electric field near the cathode face edges.[2,3] This enhanced edge emission would also explain the "W" shape of the anode groove cross-section. The computer simulations described below were conducted to test this theory.

The Simulation Code

The computer code utilized in these studies is a modified version of the DIODE2D code developed at the Naval Research Laboratory during the mid-1970's by one of the authors (R.E.L.). That original code performed numerous accurate and efficient one- and two-dimensional electrostatic diode simulations.[4,5] These results encouraged the expansion of the program to allow the full treatment of radial and axial self-magnetic fields as well as the inclusion of an imposed axial magnetic field. As in the original code, great emphasis was placed upon optimizing the numerics of the new code for use on NRL's vector machine, the Texas Instrument Advanced Scientific Computer. The coding work was completed by another of the authors (R.J.B.) in August of 1978. Since then, work to improve its efficiency has continued simultaneous to its application to a variety of problems of interest including the one presented herein. The capabilities of the code and its limitations are outlined below.

The code is 2½ dimensional, particle-in-cell (PIC). Inhomogeneities are allowed in the radial (r) and axial (z) spatial dimensions. Complete azimuthal symmetry is assumed. On the other hand, all three momentum components (r, θ, z) are retained. This retention of the theta momentum is a prerequisite for the treatment of radial and axial magnetic fields in the simulation. The "particles" in this model are axially-centered rings of

charge with all other degrees of freedom. In reality they are macroparticles carrying many times an elementary charge but retaining the physical charge-to-mass ratios of the protons and electrons which they represent. Area weighting (i.e., linear interpolation) is used to couple these charges with the electric and magnetic fields calculated over a fixed set of grid-points in the region of interest. The fields thus interpolated to the particle positions act on these charge-current rings by way of the relativistic Lorentz force equation.

The fields are treated electrostatically and magnetostatically. In this sense the code does not perform a true "simulation" since Maxwell's equations are not observed. Rather the treatment is "quasistatic". Equilibrium solutions to various diode geometries are sought. The "timesteps" which appear in the code are actually snapshots of the system while it seeks to relax toward its steady-state operation. It is this steady state which is of primary interest. In order to determine the electric field within the diode region particle charge densities are distributed over a fixed grid and the discrete Poisson's equation is solved.[6] The same technique is used to determine the axial and radial components of the self-magnetic field from the azimuthal current densities. In both cases the code permits irregular conducting boundaries inside the computational region. The treatment of such internal boundaries entails the use of a "capacitance matrix".[7] The internal surfaces thus created are held at predetermined electric potential values while magnetic flux from all but the imposed fields is excluded from them. Direct radial integration of the axial current densities over the mesh yields the azimuthal magnetic field via Ampere's Law. The outer radial boundary of the diode region may be either conducting or free-space. The electrostatic potential, ϕ, is set constant along all conducting boundaries. Along radial

free-space boundaries, ϕ is graded logarithmically and along axial ones, linearly. For A_θ, when a free-space outer radial boundary is chosen, the external source-free cylindrical vector potential eigenvectors are matched up with their internal, source-consistent counterparts there. The algorithm also permits the imposition of a temporally and spatially uniform axial magnetic field. This feature was essential to the completion of this particular study.

At the start of a typical computer run, the computational diode region is a complete vacuum, devoid of particles. The electric potential is pre-set along the entire boundary as well as along all internal conducting surfaces. A fixed value is similarly set for the imposed axial magnetic field (B_z). The emission of the ions is permitted anywhere along the conducting high voltage boundary (anode) surface. Electrons are emitted along the front face of the cathode surface. The value of the perpendicular electric field at a given emission point determines the total charge (i.e., number of particles) that will be emitted there. At the beginning of a timestep, the electric field at a surface specifies the net charge density on the surface via Gauss' Law. The surface integral of this density over a cell width around a given grid point yields the net charge which is emitted there for this timestep. Prior to the actual particle-pushing the electric field is recalculated taking into account the newly emitted charge.

The emitted particles are then pushed according to the relativistic Lorentz force law using the area weighted electric and magnetic field values interpolated at the particle position from the four nearest grid points. After the pushing in each timestep the charge and current density associated with each particle is distributed over the four nearest gridpoints using the same linear interpolation scheme in reverse. This yields a complete array of

values for the charge density, ρ, and the current density, $\vec{J}$, over the computational mesh. Poisson solving these arrays yields ϕ and A_θ from which E_R, E_z, B_R and B_z are calculated. The azimuthal component of $\vec{B}$ is obtained through direct integration of J_z over the grid. Quantities of interest are then extracted and output via diagnostic subroutines. The code then cycles to the next timestep for particle emission.

Finally, it would be noted that the numerics of the particle pushing as well as the potential solving has been completely "vectorized". Thus the momentum, position, and field components associated with the entire ensemble of particles are treated as macro-vector quantities. Arithmetic operations performed with them are accomplished in a completely vector-array format. This property of the code permits efficient running times on the most advanced scientific computers. (Of course, the interpolation of ρ, $\vec{J}$, $\vec{E}$, and $\vec{B}$ values between particle positions and grid points requires random accessing of array points and this process cannot be vectorized.)

The Computer Experiment

Configuration Under Study

The diode configuration modeled in this simulation was chosen specifically for its significant distortion of the internal electric field. Any emission enhancement resulting from this distortion should be relatively easy to see. Figure 2 provides a scale drawing of the actual geometry of the diode modeled. The hollow-cathode projects into the computational region from the left-hand boundary. A cylindrical anode cup completely surrounds it radially and to the right. One-quarter centimeter separates the cathode face from the anode disc plate while radial gap between these two coaxial electrodes is one and one-quarter centimeters wide. The cathode itself measures 1.27 centimeters in outer radius with a wall thickness of 0.14 cm. It

projects 0.08 cm into the 2-D computational region. A conducting plug fills the cathode interior to within 0.08 cm of the edge face and thus coincides with the computational region's inner left boundary. The upper half of the region's left boundary is left "open" with the electrostatic potential graded logarithmically with radius.

The vacuum diode equipotential surfaces are depicted in Fig. 3. Of particular interest in this plot is the manner in which these surfaces are compressed near the edges of the cathode face. This bunching gives rise to the electric field enhancement at these points and to the resulting enhanced electron emission there.

Operational Parameters

For all of the runs discussed herein, the diode voltage is initialized at 120 kV and climbs linearly over 50 timesteps to a steady state plateau value of 600 kV. The timestep, Δt, itself is fixed at 1.6×10^{-12} second. The two-dimensional numerical mesh over which the particles move measures 128 cells in the radial dimension and 64 cells in the axial. In addition, a monolayer of "guard cells" completely surrounds the mesh to yield a total of 130 × 66 cells overall. All boundary surfaces run between neighboring rows of gridpoints rather than along them. (Gridpoints are defined as the cell centers.) The electrostatic potentials on these boundaries are held fixed relative to the full diode potential at any given timestep throughout the simulation. The cell widths (or gridpoint spacings) are 0.0195 and 0.00521 centimeters for ΔR and ΔZ, respectively. The front face of the cathode emits electrons over six radial cells. This emission profile provided adequate resolution for this experiment. Finally, a solenoidal magnetic field is imposed and is assumed to have been on long enough to have

completely penetrated the anode and the cathode before particle emission is initiated.

For the first 300 timesteps of the simulation, only electron emission was permitted. By that time, an electrons-only steady state had been attained. The program diagnostics were then examined to determine which regions of the anode surface were being bombarded by the largest electron current densities. At timestep 301, ion emission was turned on over those regions. (In the physical diode, these are the areas where the most heating of the anode surface has occurred.)[8] The computer simulation then continues until the net ion and electron currents equilibrate. The numerical data presented in the next section are taken from this final timestep with the device in its steady-state operation.

Results

In order to gauge the specific effect of a strong imposed solenoidal magnetic field, B_z, on diode operation, the same diode was simulated with and without B_z = 30 kG. In both cases the plateau voltage is set at 600 kV. In Case 1, B_z is set equal to zero. The major phenomenum to be observed in this case is the two-dimensional electric field enhanced emission of electrons. The results are graphically presented in Fig. 4. After 300 timesteps of electrons-only operation, the equilibrium profiles of electron emission current density at the cathode face and the electron impact current density at the anode are plotted as shown. It is quite clear that the compression of electrostatic equipotential liner at the cathode face edges (see Fig. 3) has had its effect. Electron emission is up by a factor of about 2.5 at the edges as compared to the center of the cathode face. A peak electron current density of over 78 kA/cm^2 is observed at the edge. The sharpness of this profile degenerates markedly before hitting the anode face. Virtually all

of the double-peaked definition is lost. The distribution is relatively diffuse with a maximum density of only about 24 kA/cm^2. A net current of 37.6 kA now flows through the diode. Since the critical current is about 82 kA, only very weak pinching can occur.

At timestep 301, ion emission begins on the anode face in the region where the electrons have been arriving. The addition of protons into the system has a substantial effect (see Fig. 5). At equilibrium, the total current through the diode has jumped to 61.5 kA. The electron emission profile has about the same shape but it now exceeds 90 kA/cm^2 at the cathode face edges. Similarly, the anode electron impact plot is still diffuse but it now peaks at about 32 kA/cm^2. Note also that the self-pinching of the electron beam is more pronounced. The mean radius of the beam has decreased by about one millimeter in its passage across the two and a half millimeter gap.

For the diode simulation Case 2, a thirty kilogauss solenoidal magnetic field, B_z, is imposed. The results of the runs are plotted in Figs. 6 and 7. As in the previous case, only electrons flow through the system during the first 300 timesteps. Figure 6 reveals once again a double peaked emission distribution at the cathode with a maximum value of about 96 kA/cm^2. The truly dramatic change is found in the anode profile. The beam's radial diffusion while crossing the gap has been sharply restricted by the imposed B_z. The anode impact plot has about the same shape as the plot of the electron emission. It peaks at about 83 kA/cm^2. In this steady state about 40 kA is flowing through the diode. The results become more marked after ions are permitted into the system (see Fig. 7). Peak electron emission rises to 108 kA/cm^2 while a maximum of 92 kA/cm^2 of electron current density is being deposited at the anode face. (Note that the total diode current is

59.2 kA in steady state. This is less than that recorded for the $B_z = 0$ case for the simple reason that ion emission was artifically limited to fewer points on the anode face for this run.)

These results indicate the following: (a) Electron emission is enhanced at the cathode face edges. (b) Protons flowing in the system substantially increase net diode current figures. (c) A strong imposed B_z significantly reduces the self-pinching of the electron beam as well as its radial diffusion.

Comparison of Results to Theory and Experiment

The computational results just presented gain significance only through comparison with the predictions of theory as well as with the findings of experiment. The first question is that of electron emission enhancement due to two-dimensional electric field distortions. In a one-dimensional analysis, in the absence of ions the Child-Langmuir emission law predicts that for an infinite flat plate vacuum diode with gap separation, d (in centimeters), and potential difference, V (in volts), electrons will be emitted uniformly over its cathode surface with a current density[9] of

$$J_{CL} = 2.34 \times 10^{-6} V^{3/2} d^{-2}$$

For the diode treated in this paper, V equals 600 kV while d is 0.25 centimeters. The formula thus yields $J_{CL} \approx 17.4$ kA/cm^2. This prediction comes fairly close to the 20-24 kA/cm^2 measured near the center of the cathode face. One would physically expect those interior regions to most closely resemble the one-dimensional model. At the edges, on the other hand, the electron emission exceeds the one-dimensional J_{CL} prediction by a factor of 4 to 5.

The introduction of protons into the system modifies the theoretical predictions. This new condition is termed one-dimensional bi-polar flow. The new electron emission current density, J_{BP}, is approximated by

$$J_{BP} \approx 1.86\ J_{CL}$$

Thus, it predicts about 32 kA/cm^2 for the diode operating with ions and electrons. This agrees quite well with the 32-42 kA/cm^2 seen in the simulation for the inner cathode face emission. However, it is off by a factor of 2.5 to 3 from the edge emission figures. The two-dimensional field enhancement effects have to drastically change the physics there from the simple 1-D analysis.

The second major question concerns the effect of the 30 kilogauss solenoidal magnetic field on the electron current densities impacting the anode face. Experimental corroboration for the computational results presented herein was derived from the previously mentioned observations obtained from a series of runs by the Gamble I device at NRL in the mid 1970's. These empirical results were presented by Cooperstein to the 1976 meeting of the Plasma Physics Division of the American Physical Society. Of those results, one of particular interest here is shown in Fig. 8. Using a diode configuration closely approximating that modeled in this computer simulation, a double peaked damage pattern was observed on the anode face at very nearly the radius of the hollow cathode after each discharge. Such damage could result if the anode material was being pulverized by the electron beam. The pulverization of carbon requires the deposition of 2 kcal/g. Assuming a mean graphite density of 2.5 j/cc this translates to 5 kcal/cc. The electron beam in the computer simulation was delivering a peak power of 54 j/cm^2-sec over an area of roughly 1.1 cm^2. Thus the experimentally observed damage could

be obtained to a depth of about one millimeter if the simulated beam were maintained for approximately forty nanoseconds. According to Fig. 8, the experimental voltage and current peaks were 1 MV and 200 kA, respectively. Comparing this to the 600 kV and 60 kA of the simulation would indicate that the experimental diode could have achieved the observed damage in twenty nanoseconds or less.

In short, the correlation between experiment and simulation is very good. The empirical results can now be better understood as a consequence of the combined effects of two-dimensional electric field electron emission enhancement as well as of the electron path stiffening caused by the strong axial magnetic field.

References

1. G. Cooperstein, D. A. Hammer, I. M. Vitkovitsky, S. J. Stephanakis, J. J. Condon, and Shyke A. Goldstein, Bulletin of the American Physical Society, San Francisco, 1976, p. 1096.
2. Edward Ott, Thomas M. Antonsen, Jr., R. V. Lovelace, Phys. Flu. 20, 1180 (1977).
3. J. Chen and R. V. Lovelace, Phys. Flu. 21, 1623 (1976).
4. S. A. Goldstein, R. C. Davidson, J. G. Siambis, and Roswell Lee, Phys. Rev. Lett. 33, 1471 (1974).
5. Shyke A. Goldstein and Roswell Lee, Phys. Rev. Lett. 35, 1079 (1975).
6. Robert J. Barker, Banach Center Publications 3, 255 (1975), Warsaw, Poland.
7. B. L. Buzbee, F. W. Dorr, and J. A. George, Technical Report CS-71-195, Computer Science Department, Stanford University, Stanford, California (1970).
8. Shyke A. Goldstein, G. Cooperstein, Roswell Lee, D. Mosher, and S. J. Stephanakis, Phys. Rev. Lett. 40, 1504 (1978).
9. Robert K. Parker, Technical Report AFWL-TR-73-92, USAF Weapons Lab., Albuquerque, New Mexico (1973).

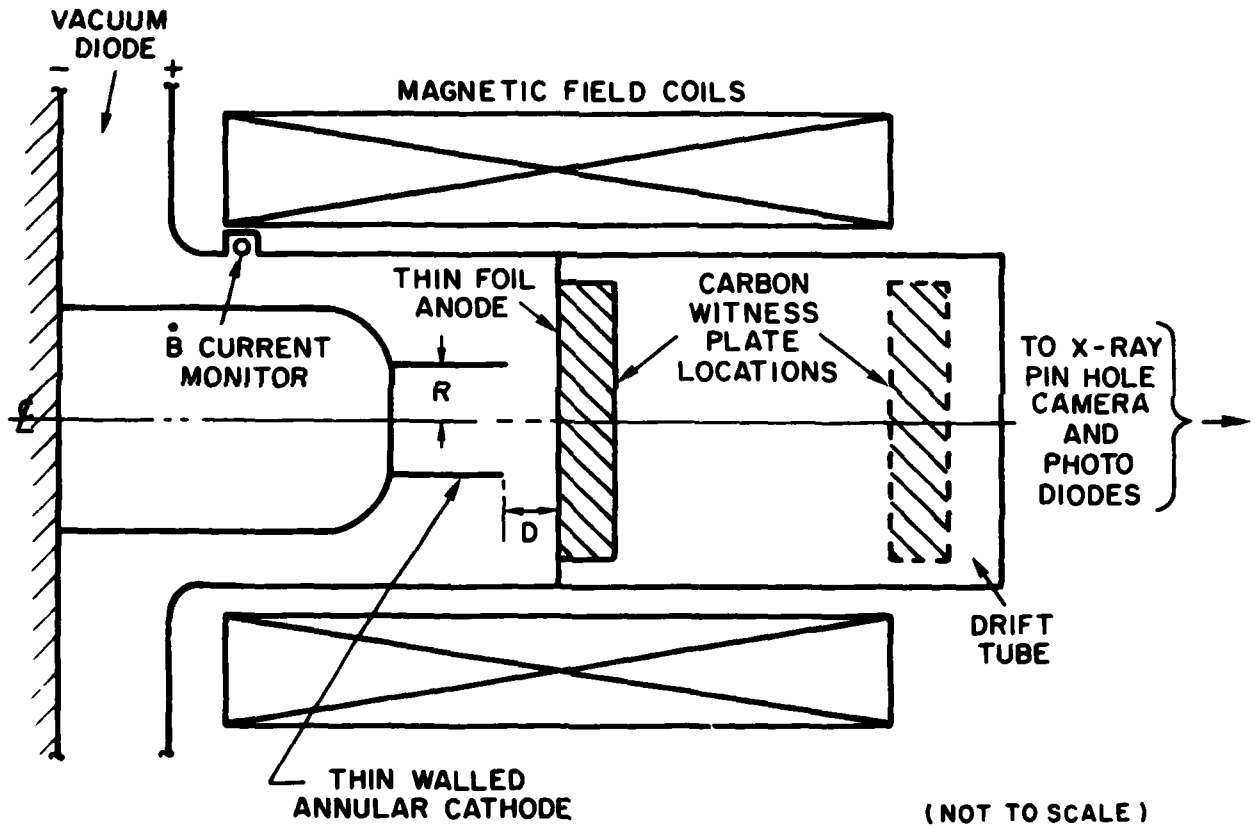

Fig. 1 - Experimental arrangement

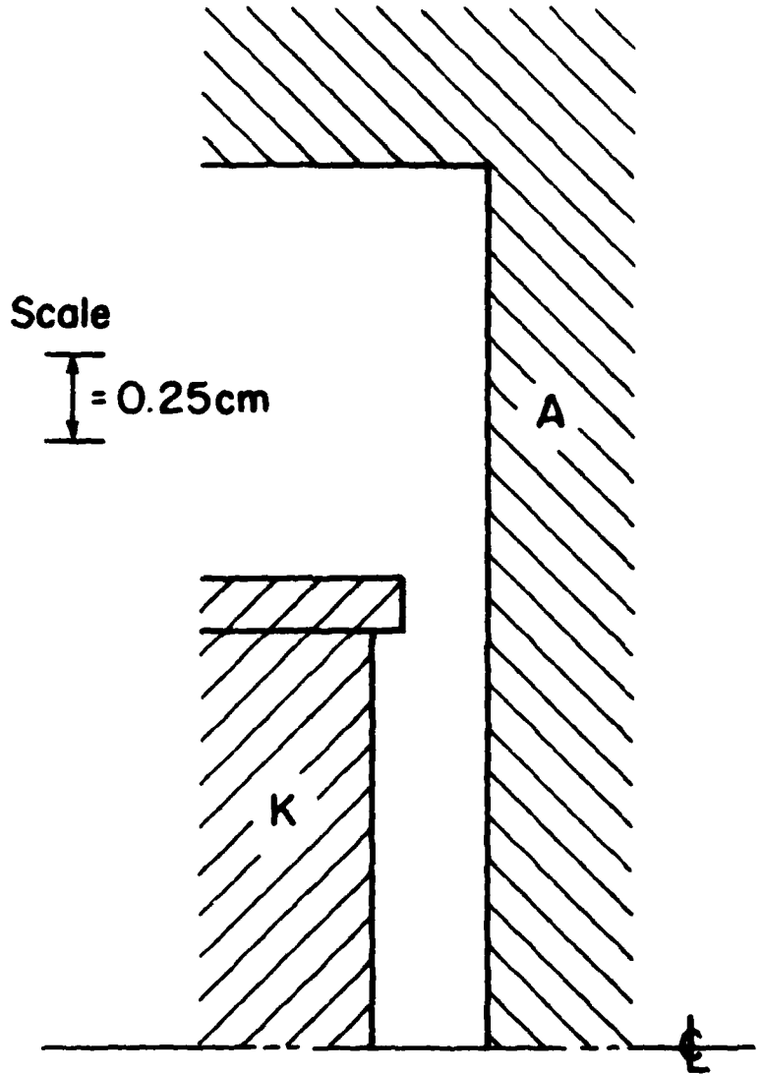

Fig. 2 - Scale drawing of diode

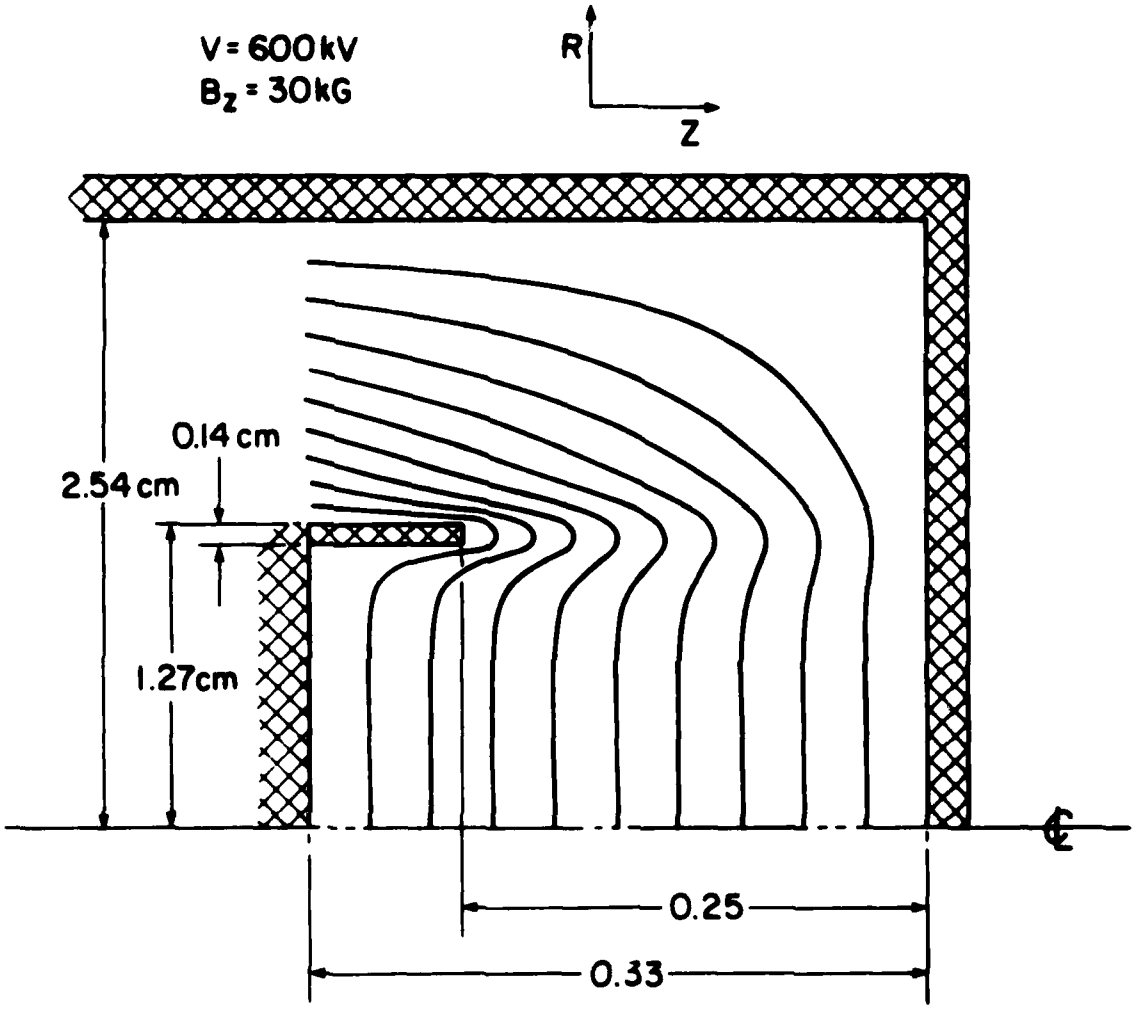

Fig. 3 - Vacuum equipotential plot

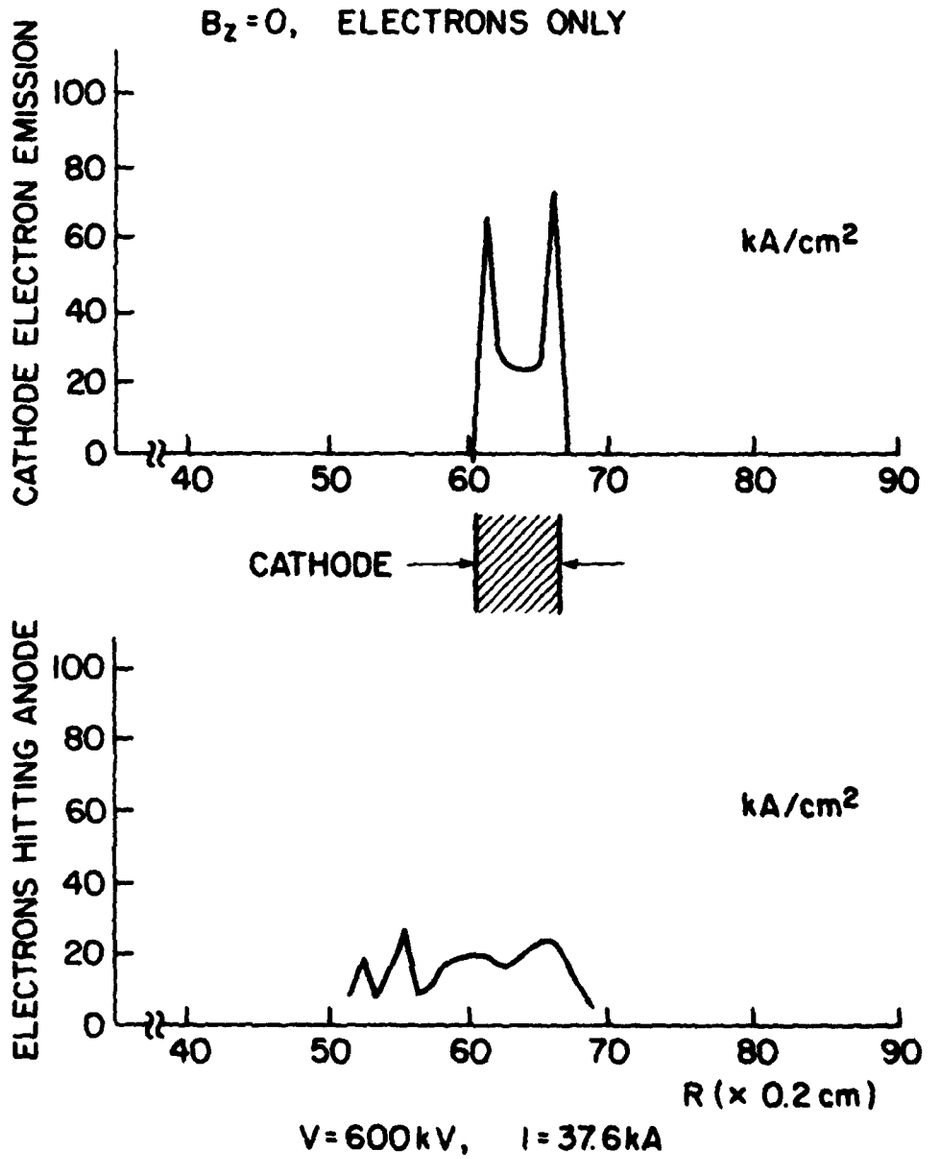

Fig. 4 - Steady-state current density for case 1 with only electrons

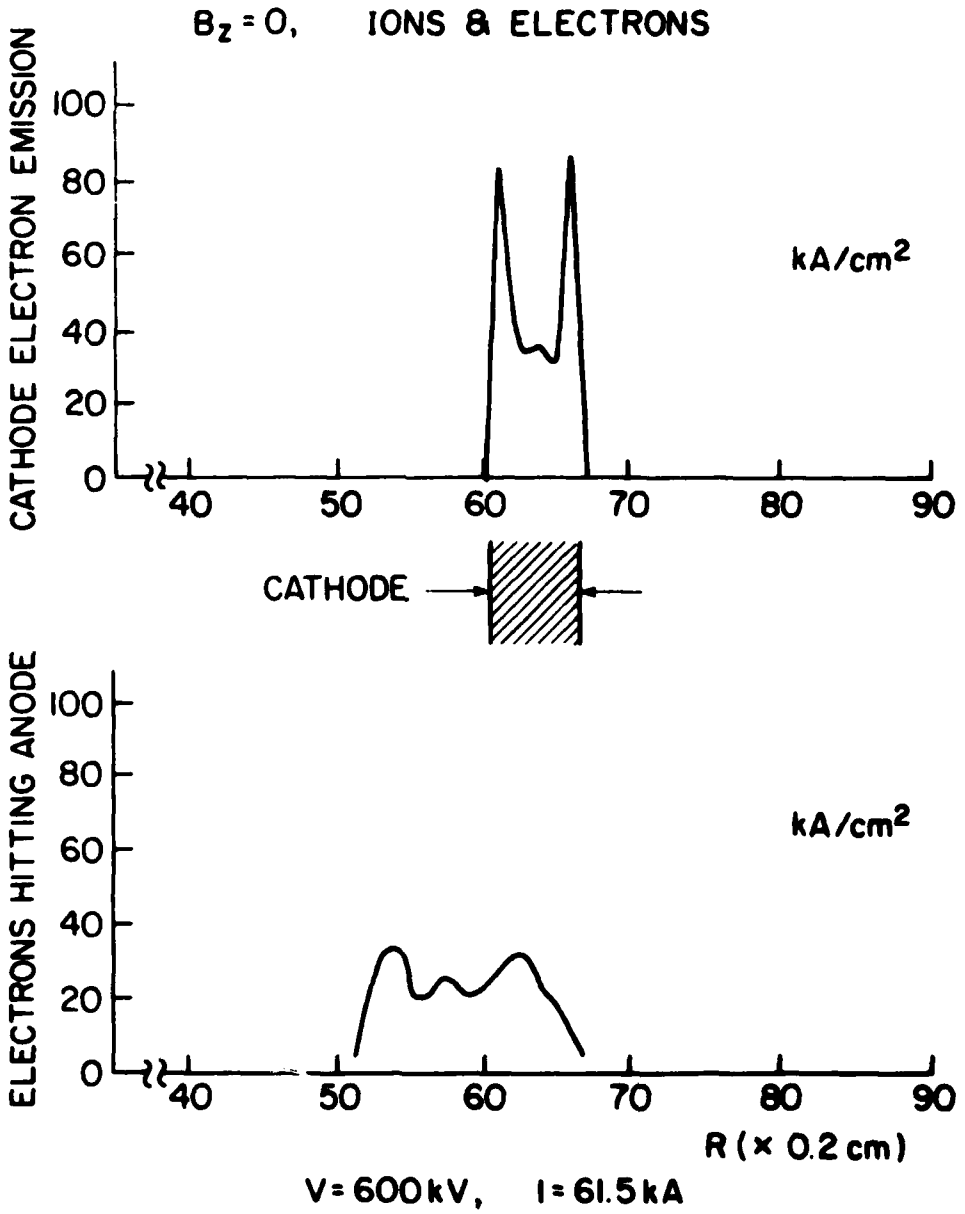

Fig. 5 - Steady-state current density for case 1 with electrons and ions

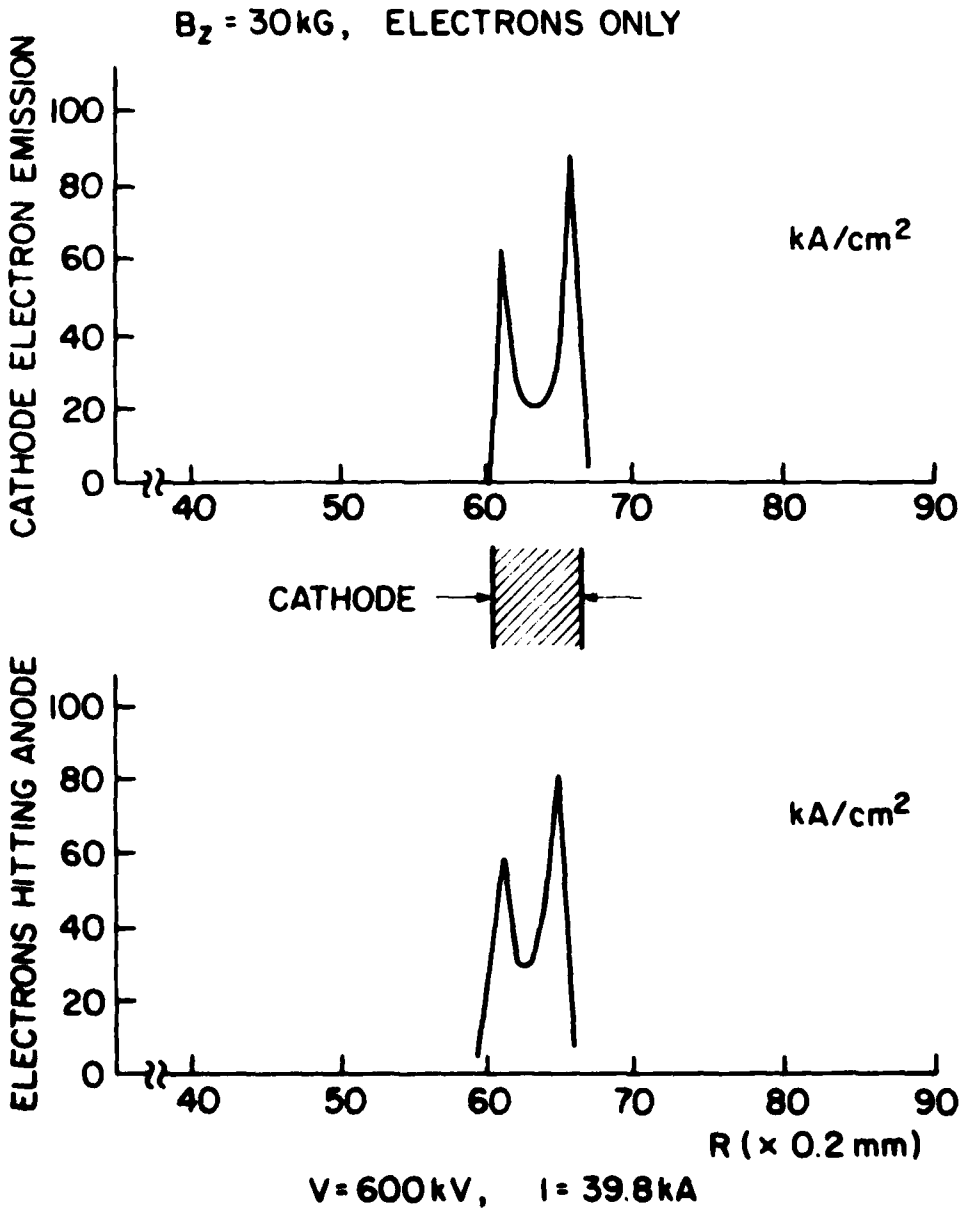

Fig. 6 - Steady-state current density for case 2 with only electrons

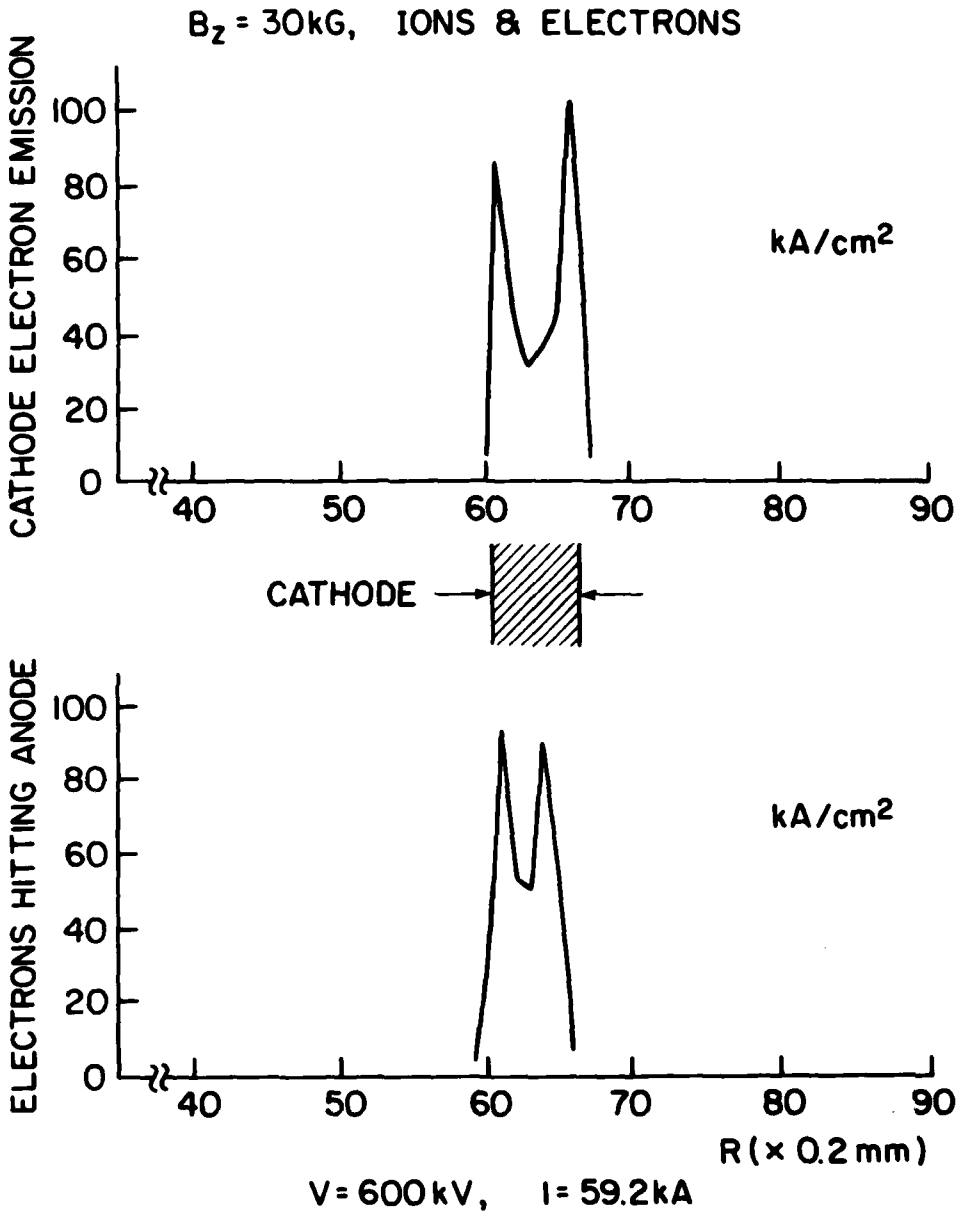

Fig. 7 - Steady-state current density for case 2 with electrons and ions

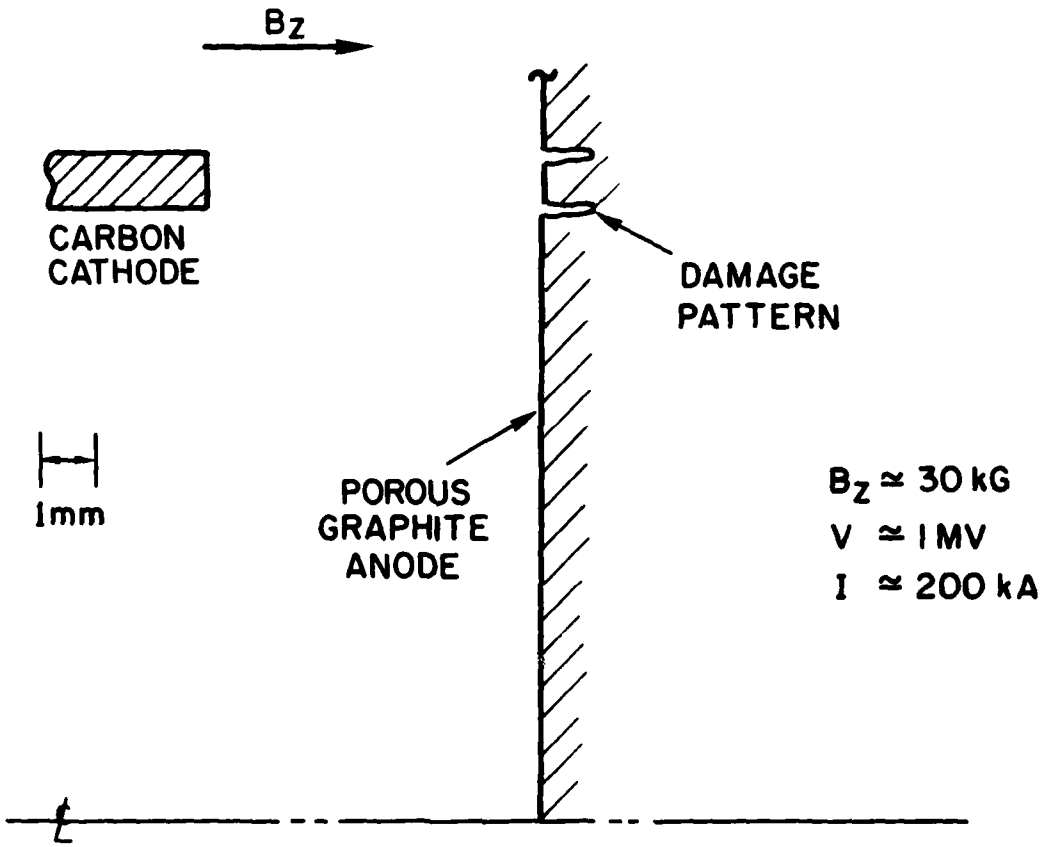

Fig. 8 - Witness plate damage

DISTRIBUTION LIST

U.S. Department of Energy
P. O. Box 62
Oak Ridge, Tennessee 37830 (50 copies)

National Technical Information Service
U.S. Department of Commerce
5285 Port Royal Road
Springfield, VA 22161 (24 copies)

U.S. Department of Energy
Division of Inertial Fusion
Washington, D. C. 20545

Attn: G. Canavan (2 copies)
T. F. Godlove (1 copy)

Defense Technical Information Center
Cameron Station
5010 Duke Street
Alexandria, VA 22314 (12 copies)

Director
Defense Nuclear Agency
Washington, D. C. 20305

Attn: R. L. Gullickson (1 copy)
J. Z. Farber (1 copy)

Lawrence Livermore Laboratory
P. O. Box 808
Livermore, CA 94550

Attn: R. J. Briggs (1 copy)
R. O. Bangerter (1 copy)
J. H. Nuckolls (1 copy)
S. S. Yu (1 copy)
E. P. Lee (1 copy)

Sandia Laboratories
P. O. Box 5800
Albuquerque, NM 87115

Attn: G. Yonas (1 copy)
G. W. Kuswa (1 copy)
J. R. Freeman (1 copy)
D. J. Johnson (1 copy)
P. A. Miller (1 copy)
J. P. Quintenz (1 copy)
J. P. Vandevender (1 copy)
S. Humphries (1 copy)

Los Alamos Scientific Laboratory
P. O. Box 1663
Los Alamos, NM 87545

Attn: R. B. Perkins (1 copy)
L. E. Thode (1 copy)
R. J. Faehl (1 copy)

University of California
Lawrence Livermore Laboratory
Berkeley, CA 94720

Attn: D. Keefe (1 copy)

Argonne National Laboratory
9700 South Cass Avenue
Argonne, Illinois 60439

Attn: R. J. Martin (1 copy)

Brookhaven National Laboratory
Upton, New York 11973

Attn: J. R. Powell (1 copy)

National Science Foundation
Mail Stop 19
Washington, D. C. 20550

Attn: D. Berley (1 copy)
R. M. Sinclair (1 copy)

Air Force Weapons Laboratory, AFSC
Kirtland AFB
Albuquerque, NM 87117

Attn: D. C. Straw (1 copy)
H. Dogliani (1 copy)
B. Hanson (1 copy)

Harry Diamond Laboratories
Adelphi, Maryland 20783

Attn: S. Graybill (1 copy)

Cornell University
Ithaca, NY 14850

Attn: J. Nation (1 copy)
D. A. Hammer (1 copy)

National Bureau of Standards
Washington, D. C. 20234

Attn: J. Leiss (1 copy)

Stevens Institute of Technology
Castle Point Station
Hoboken, New Jersey 07030

Attn:	W. H. Bostick	(1 copy)
	V. Nardi	(1 copy)
	M. Seidl	(1 copy)

Institute for Plasma Research
Stanford University
Stanford, CA 94305

Attn:	O. Buneman	(1 copy)
	K. Harker	(1 copy)
	D. Illic	(1 copy)
	R. J. Vidmar	(1 copy)

Lawrence Berkeley Laboratory
University of California
Berkeley, CA 94720

Attn:	C. K. Birdsall	(1 copy)
	Y. Matsuda	(1 copy)
	A. Sternlieb	(1 copy)

Department of Physics
U. S. Air Force Academy
Colorado Springs, Colorado 80840

Attn:	D. Murawinski	(1 copy)

University of California
Irvine, CA 92664

Attn:	G. Benford	(1 copy)
	N. Rostoker	(1 copy)

JAYCOR
205 S. Whiting Street
Alexandria, VA 22304

Attn:	D. A. Tidman	(1 copy)
	J. Guillory	(1 copy)
	R. Hubbard	(1 copy)

JAYCOR
1401 Camino Del Mar
Del Mar, CA 92014

Attn:	E. Wenaas	(1 copy)

JAYCOR
360 S. Hope Avenue
Santa Barbara, CA 93105

Attn:	W. E. Hobbs	(1 copy)
	S. S. Wang	(1 copy)

Maxwell Laboratories, Inc.
9244 Balboa Avenue
San Diego, CA 92123

Attn:	A. C. Kolb	(1 copy)
	P. Korn	(1 copy)
	J. Pearlman	(1 copy)
	R. W. Clark	(1 copy)

Mission Research Corporation
1400 San Mateo Blvd. SE
Albuquerque, NM 871108

Attn:	B. B. Godfrey	(1 copy)

Physics International Co.
2700 Merced Street
San Leandro, CA 94577

Attn:	S. D. Putnam	(1 copy)
	A. J. Toepfer	(1 copy)
	P. W. Spence	(1 copy)
	J. Benford	(1 copy)
	R. Genuario	(1 copy)
	J. Maenchen	(1 copy)
	B. Bernstein	(1 copy)
	E. B. Goldman	(1 copy)

R&D Associates
P. O. Box 9695
Marina Del Ray, CA 90291

Attn:	E. Martinelli	(1 copy)

Weizmann Institute of Science
Rehovot, Israel

Attn:	A. E. Blaugrund	(1 copy)
	Z. Zinamon	(1 copy)
	E. Nardi	(1 copy)

Institut Fur Neutronenphysik
un Reaktortechnik
Postfach 3640, Kernforschungszentrum
D-7500 Karlshruhe 1, Germany

Attn:	H. N. Karow	(1 copy)
	W. Schmidt	(1 copy)

Max-Planck-Institut
fur Plasmaphysik
8046 Garching bei Munchen
West Germany

Attn: R. Lengyel (1 copy)

Nuclear Physics Institute
Novosibirsk-90
630090 USSR

Attn: Yu. Rosenraukh (1 copy)
V. G. Davidovski (1 copy)
D. Ryutov (1 copy)

Lebedev Physical Institute
Leninsky Prospect 53
Moskow, USSR

Attn: O. Semenov (1 copy)
V. Gribkov (1 copy)
V. H. Papadichev (1 copy)
A. A. Kolomensky (1 copy)
A. N. Lebedev (1 copy)

Institute of Nuclear Physics
P. O. Box 25
Tomak 50, USSR

Attn: V. M. Bistritsky (1 copy)

Physico-Technical Institute
Academicheskaya, 1
Kharkov 108, USSR

Attn: B. I. Ivanov (1 copy)

I. V, Kurchatov Institute of Atomic Energy
46 Ulitsa Kurchatov
P. O. Box 3402
Moscow D-182, USSR

Attn: L. Rudakov (1 copy)
V. Smirnov (1 copy)

Technical University of Prague
Brehova 7 - PRAHA 1
Czechoslovakia

Attn: L. Drska (1 copy)

Stanford University
SLAC
P. O. Box 4349
Stanford, CA 94305

Attn: W. B. Herrmannsfeldt (1 copy)

University of Illinois
Urbana, Illinois 61801

Attn: G. H. Miley (1 copy)

Mission Research Corporation
735 State Street
Santa Barbara, CA 93101

Attn: C. L. Longmire (1 copy)

Systems, Science and Software
P. O. Box 1620
La Jolla, CA 92038

Attn: A. Wilson (1 copy)

Institute of Laser Engineering
Osaka University
Yamadakami, Suita
Osaka 565, Japan

Attn: S. Nakai (1 copy)
K. Imasaki (1 copy)

CEA, Centre de Etudes de Lemeil
B. P. 27
94190 Villeneuve, Saint George
France

Attn: A. Jolas (1 copy)

CEA, Centre de Etudes de Valduc
B.P. 14
21120 Is-sur-Tille
France

Attn: C. Patou (1 copy)
C. Peugnet (1 copy)
M. Roche (1 copy)
N. Camarcat (1 copy)
C. Bruno (1 copy)
J. Barbaro (1 copy)

Ecole Polytechnique
Labo, PMI
91128 Palaiseau Cedex
France

Attn: H. Doucet (1 copy)
J. M. Buzzi (1 copy)

Institut d'Electronique Fondamentale
Universite' Paris Xl-Bat. 220
F91405 Orsay
France

Attn: G. Gautherin (1 copy)

Physical Research Laboratory
Navrangpura
Ahmedabad - 380009, India

Attn: V. Ramani (1 copy)

Shivaji University
Kolhapur, India

Attn: L. N. Katkan (1 copy)

Bhabha Atomic Research Centre
Bombay - 400085, India

Attn: B. K. Godwal (1 copy)
A. S. Paithankar (1 copy)

Instituto De Investigaciones Cientificas Y Technicas
De Las Fuerzas Armadas
Zufriategui y Varela
V. Martelli 1603
Pcia Bs. As. - R. Argentina

Attn: N. B. Camusso (1 copy)

Institute of Atomic Energy
Academia Sinica - Peking
People's Republic of China

Attn: R. Hong (1 copy)

Naval Research Laboratory
Attn: Code 2628
Washington, D. C. 20375 (25 copies)

Naval Research Laboratory
Attn: Code 4040
Washington, D. C. 20375 (1 copy)

Naval Research Laboratory
Attn: Code 6682
Washington, D. C. 20375 (1 copy)

Naval Research Laboratory
Attn: Name/Code
Washington, D. C. 20375

Addressee:
Code 4700 (25 copies)
Code 4707 - Dr. J. Davis (1 copy)
Code 4730 - Dr. S. Bodner (1 copy)
Code 4740 - Dr. V. Granatstein (1 copy)
Code 4760 - Dr. B. Robson (1 copy)
Code 4761 -
Code 4770 - Mr. I. Vitkovitsky (1 copy)
Code 4771 - Dr. D. Mosher (1 copy)
Code 4773 - Dr. G. Cooperstein (1 copy)
Code 4790 - Dr. M. Lampe (1 copy)
Dr. I. Haber (1 copy)
Dr. D. Colombant (1 copy)
On-Site Contractors:
Code 4770 - Dr. R. Barker (25 copies) (Jaycor)
Dr. S. Goldstein (1 copy) (Jaycor)